

Vibration reduction on circular saw blades with vibroacoustic metamaterials

Sebastian RIEß¹*, William KAAL¹, and Sven HEROLD¹

Fraunhofer Institute for Structural Durability and System Reliability LBF, 64298, Darmstadt, Germany

Abstract. The presented work focuses on the experimental investigation of a vibroacoustic metamaterial integrated into a spinning circular saw blade. Vibroacoustic metamaterials are a novel technology for broadband vibration reduction. Built from an array of local resonators, a broadband vibration reduction characteristic in the frequency domain (a so-called stop band) can be achieved. A design of a vibroacoustic metamaterial suitable for integration into a circular saw blade is developed and a numerical stop band prediction is performed. The resonators of the vibroacoustic metamaterial are integrated into the saw blade with a water jet cutting machine to create slots, forming flaps that are free to oscillate. The structural dynamic behavior of the saw blade with integrated vibroacoustic metamaterial is experimentally investigated on a rotor dynamic test bench and compared to that of a standard saw blade. The saw blades are excited by an automatic impulse hammer and the resulting out-of-plane vibrations are measured with a laser vibrometer at two different radii. Measurements are conducted at different rotational speeds up to 1800 rpm. Up to rotational speeds of 1000 rpm a stop band characteristic in the frequency range of 1900–2500 Hz is observed.

Key words: circular saw blade; vibroacoustic metamaterial

1. INTRODUCTION

Circular saw blades are widely used in industry and construction because of their high cutting speeds, ease of handling, and the mobility of the sawing machine. Due to their thin-walled disk shape such saw blades are prone to vibrations excited by the sawing process. These vibrations are the predominant source of the disturbing noise during sawing [1], which affects both the workers and people in the wider environment and makes health and safety measures necessary. State-of-the-art measures to reduce saw blade vibrations and noise are the integration of damping slots [2–4], sandwich-like configurations where a damping layer is integrated into the saw blade [5–7], the optimization of the saw teeth [1] as well as the integration of radial slots at the circumference of the saw blade [8–10]. The effect of slots in the saw blade is attributed to the shift of eigenfrequencies, the split of eigenmodes, the relative movement of segments leading to damping (if the slot is filled with a damping material or sawdust), and the suppression of free wave propagation [4]. While sandwich saw blades are highly effective for noise reduction, they are comparatively expensive since they are built from multiple parts. The optimization of saw teeth is a promising approach, but it is achieved by reducing the size of the teeth leading to smaller saw dust particles which may potentially lead to cancer [11]. Saw blades with slots are widely used in industry but have limited effectiveness in terms of noise reduction.

Vibroacoustic metamaterials (VAMM) with local resonators are a novel technology for vibration reduction, especially

promising for thin-walled, broad structures. They consist of an ordered array of local resonators, which results in a vibration reduction in a certain frequency region, called a stop band. The suitability of VAMM was shown in various applications like airplane cabins [12], cars [13], and industrial machines [14] for out-of-plane vibration suppression. In terms of rotor dynamics, metamaterials are being investigated for the torsional [15] and lateral vibration reduction [15, 16] of rotors. The out-of-plane vibration reduction of spinning disk-like structures using metastructures was investigated numerically in the non-rotating state [17]. In a prior work of the author [18] a saw blade was modified with a VAMM and experimentally analyzed in the non-rotating state.

The present work extends the state of the art through the experimental investigation of a disk-like rotor (saw blade) with an integrated locally resonant VAMM for out-of-plane vibration reduction in the rotating state. For this, a VAMM design suitable for a saw blade is developed and numerically designed. After that, the saw blade is manufactured and characterized in terms of its structural dynamics with the help of a laser vibrometer on a rotor dynamic test bench. The leading research question is whether the stop band and its characteristics are still preserved in the rotating state.

2. VIBROACOUSTIC METAMATERIALS

VAMMs with local resonators are a recent technology for vibration reduction, capable of inducing stop band behavior for vibrations in the frequency domain. They consist of an array of distributed mechanical resonators, which are placed at intervals smaller than half the wavelength of the vibration that is to be reduced. The resonators are all tuned to the same resonant frequency. A schematic VAMM along with an exemplary stop band can be seen in Fig. 1.

*e-mail: sebastian.riess@lbf.fraunhofer.de

Manuscript submitted 2023-05-05, revised 2023-09-17, initially accepted for publication 2023-10-13, published in December 2023.

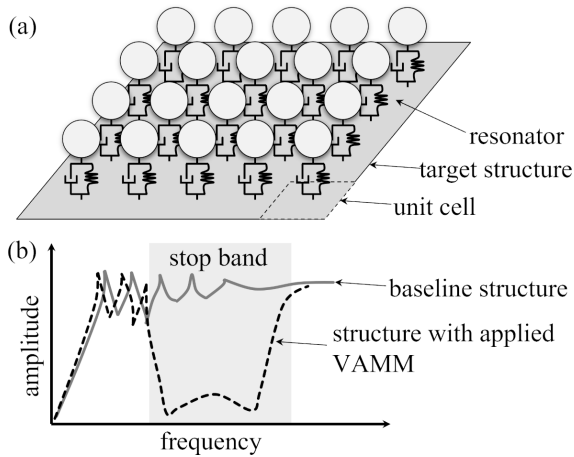


Fig. 1. (a) Schematic of a VAMM, (b) exemplary stop band in the frequency domain

Applying Bloch's theorem [19], the stop band behavior of an infinite, periodic VAMM can be predicted by calculating the dispersion curve of a single unit cell (see Fig. 1a). A unit cell is the smallest undividable unit of a VAMM, consisting of a mechanical resonator and a section of the host structure. The stop band starting frequency is given by the resonant frequency of the resonator. The width of the stop band is dependent on the oscillating mass and damping. Further information on VAMMs can be found in [20].

3. REQUIREMENTS AND SETUP

To investigate the possible vibration and noise reduction by a VAMM on a rotating saw blade, both a saw and a saw blade for modification need to be chosen. The saw blade chosen for this study has a diameter of 305 mm, a central bore of 30 mm, a thickness of 1.8 mm, a cutting width of 2.3 mm, and 40 hard metal teeth. It was chosen because it has a common diameter representing many saw blades used in workshops for cutting wood. In addition, the same manufacturer has a geometrically identical saw blade, acoustically optimized utilizing damping slots, which can be used as a benchmark for performance comparison with the VAMM blade. For future investigations, this saw blade can provide a benchmark. For a saw machine, a chop saw was chosen. This kind of saw can easily be automated to be able to do tests remotely, without having to be in the same room for safety reasons.

To set a frequency range for the stop band, acoustic measurements of the sawing process of beech wood were performed with a sound camera. The setup, as well as the sound spectrum, can be seen in Fig. 2. The first-order excitation at idling (approximately 2400 Hz and 3600 rpm) drops to approximately 2000 Hz because of the high load during sawing under full load conditions. To reduce the sawing noise, this frequency range was chosen as the desired stop band range. Furthermore, the human ear is highly sensitive around this frequency range. The large amplitude at approximately 650 Hz does not change with respect to the rotational speed and is therefore most likely due to a resonance of the housing of the saw machine.

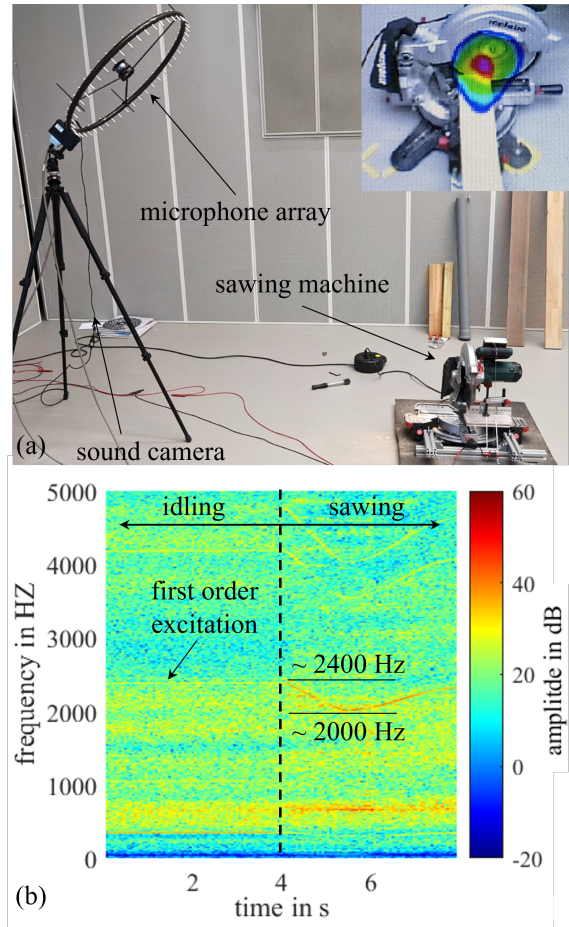


Fig. 2. (a) Set up of the acoustic measurement of the sawing process and (b) measured acoustic spectrum while idling and sawing

The close-up picture of the sound camera at the top right corner of Fig. 2a shows that the predominant noise emission can be attributed to the saw blade. The largest emissions are concentrated at a position close to the sawing process.

4. NUMERICAL DESIGN OF THE SAW BLADE WITH A VIBROACOUSTIC METAMATERIAL

To design a VAMM suitable for the saw blade, an experimentally validated numerical finite element (FE) model of the saw blade was developed. By model updating, the material parameters of the saw blade were identified. With the obtained material parameters, the unit cell was designed. The stop band prediction was done both on a unit cell level for infinite boundary conditions as well as for the saw blade structure with finite dimensions.

4.1. Numerical model of the saw blade

The FE model with free velocity boundary conditions, together with a picture of the parameters that need to be updated, are shown in Fig. 3. The diameters $d_{rt,i}$ and $d_{rt,o}$ refer to a roll tensioning ring. Roll tensioning shifts up the eigenfrequencies especially in the lower frequency range below 500 Hz to enlarge the critical speed. The model was created in Ansys Workbench

and consists of 18 361 quadratic elements with six degrees of freedom. Within a diameter of 274 mm, hexahedron elements (SOLID186) were used. The tooth region was meshed using tetrahedral elements (SOLID187) due to the more complex geometry of the teeth.

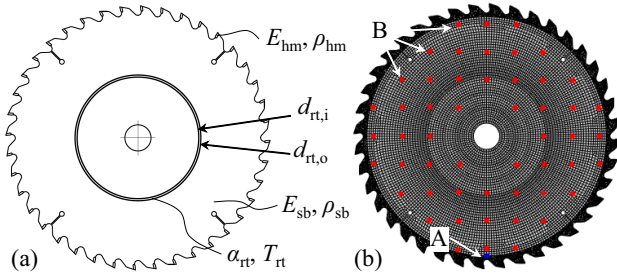


Fig. 3. (a) Model parameters, (b) FE-Model of the saw blade

The saw blade structure is excited with an impulse force at point A (blue). The averaged acceleration output is derived from point B (red). For validation of the numerical model, measurement of the saw blade was conducted suspended on foam, to ensure a free velocity boundary condition. The surface velocity was measured with a laser-vibrometer at the same points as indicated in Fig. 3b. For excitation, an automatic modal hammer was used.

To fit the simulation and the experimental data, the Young's Modulus E and density ρ of the saw blade and the hard metal teeth were updated. To account for the tension ring, the diameters $d_{rt,i}$ and $d_{rt,o}$ have to be identified. The prestress through rolling is modeled as thermal stress. For that, the temperature T_{rt} and the coefficient of thermal expansion α_{rt} are altered. A good agreement of the simulation and measurement data was obtained for $E_{sb} = 210$ GPa, $\rho_{sb} = 7925$ kg/m³ for the saw blade, $E_{hm} = 650$ GPa and $\rho_{hm} = 14000$ kg/m³ for the hard metal teeth and $d_{rt,i} = 130$ mm, $d_{rt,o} = 135$ mm, $\alpha_{rt} = 0.00018$ 1/K and $T_{rt} = 40^\circ\text{C}$ for the roll tensioning ring (Fig. 4).

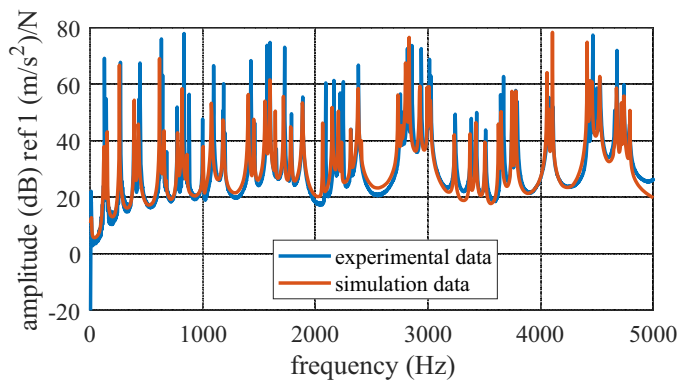


Fig. 4. Averaged acceleration transfer functions of the model and experiment

4.2. Numerical design of the unit cell

Because it is not possible to glue resonators to the saw blade like for example in [12], since this would affect the sawing process and damage the resonators while sawing, the resonators

must be integrated into the saw blade using a cutting process. A VAMM with resonators being cut into the host structure was demonstrated by AL BA'BA'A *et al.* in [21] and already applied to a saw blade in a previous study of the author in [18]. Since the objective of the present work is to investigate the behavior of a saw blade with incorporated VAMM in the rotating state, the unit cell concept already developed and validated in [18] (see Fig. 5) was chosen and adapted to the new saw blade. As was seen in sawing tests with the saw blade developed in [18], the resonators have no negative impact on the cutting quality. The teeth of a saw blade are usually entangled or are wider than the main body of the saw blade. This gives the resonators some space to oscillate in the axial direction (referring to the rotational axis of the saw blade). For the saw blade chosen for modification in this work, this gap is 0.25 mm in both directions.

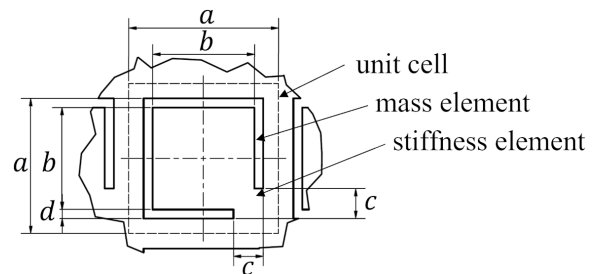


Fig. 5. A resonator cut into the saw blade structure with geometric parameters

The marked parameters a (width of the unit cell), b (width of mass), c (width of spring element), and d (groove width) in Fig. 5 need to be tuned to achieve the targeted stop band behavior.

The size of the unit cell needs to be smaller than half the wavelength of the vibration at the stop band starting frequency f [20]. Referring to Kirchhoff plate theory, the wavelength λ in a plate with Young's Modulus E , density ρ , thickness t , and Poisson's ratio ν is given by equation (1)

$$\lambda = \sqrt[4]{\frac{(2\pi)^2}{f^2} \frac{t^2 E}{12\rho(1-\nu^2)}}. \quad (1)$$

With the mechanical parameters from Section 4.1, a Poisson's ratio of $\nu = 0.33$ and a stop band starting frequency of $f = 2000$ Hz, a wavelength λ of approximately 94 mm is obtained. Therefore, the unit cell width a , needs to be smaller than 47 mm. The groove size d was set to 1 mm, which is approximately the smallest groove that can be cut into the saw blade with the water jet cutting machine available at the experimental facility used for this study. Larger groove sizes were not applied, in order to not excessively weaken the saw blade. The other parameters, a , b , and c were varied in terms of parameter variation. A good parameter set satisfying the requirements regarding the stop band range was found for $a = 24$ mm, $b = 16$ mm, $c = 4.5$ mm, and $d = 1$ mm. Using Bloch's theorem [19], the characteristic wave propagation in the periodic

system of an infinite resonator array can be analyzed for a single unit cell. In an undamped system, stop bands can be identified as frequency regions where no free wave propagation is possible. In Fig. 6d the unit cell in its first eigenmode and the investigated propagation directions θ of 0° , 45° and 90° are shown. Figure 6a–c shows the dispersion curves for the different propagation directions. Depending on the direction of propagation, the location and width of the stop band is found to change. The 0° and 90° directions show stop bands at 1690–2720 Hz and the 45° direction shows a stop band at 1850–2700 Hz. Independent of the propagation direction, the desired stop band range of 2000–2400 Hz is achieved.

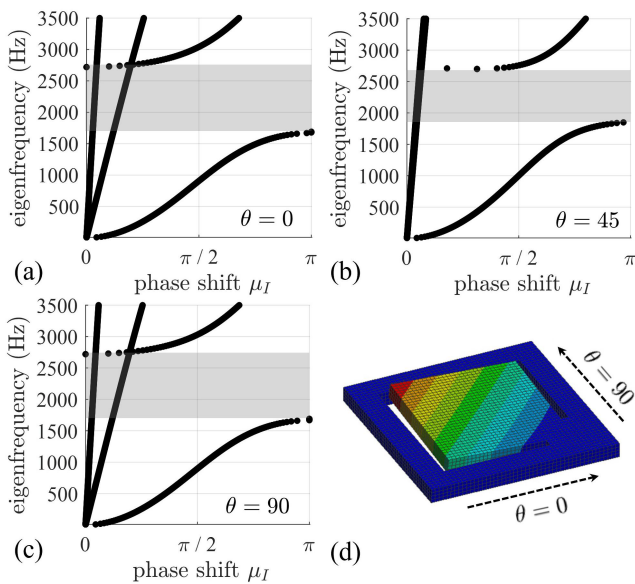


Fig. 6. (a–c) Dispersion curves with stop bands (grey) for propagation directions $\theta = 0^\circ$, $\theta = 45^\circ$ and $\theta = 90^\circ$, (d) unit cell in 1st eigenmode

When rotating, a centrifugal force acts on the saw blade having a stiffening effect. The same happens to the unit cell, which might lead to a detuning of the eigenfrequency of the resonators. As indicated by equation (2), the centrifugal force F_{cf} is dependent on the radius r . The mass is denoted by m and ω is the rotational speed

$$F_{cf} = m\omega^2 r. \quad (2)$$

Since the unit cells are placed at different radii and orientations to form a regular array, the stiffening effect is different for each unit cell. This might lead to a detuning of the resonators, which can affect the functionality of a VAMM. To investigate this effect, numerical simulations of the unit cell in different angular orientations subjected to a rotational speed of 380 rad/s (3628.7 rpm, approximately the idling speed of the saw machine) placed at three different radii ($r = 50, 100, \text{ and } 150 \text{ mm}$) away from the axis of rotation were performed (see Fig. 7a). The results, as presented in Fig. 7b show that the detuning of the eigenfrequency is expected to be below 0.5%. This detuning is lower than the expected detuning caused by production tolerances and can therefore be neglected.

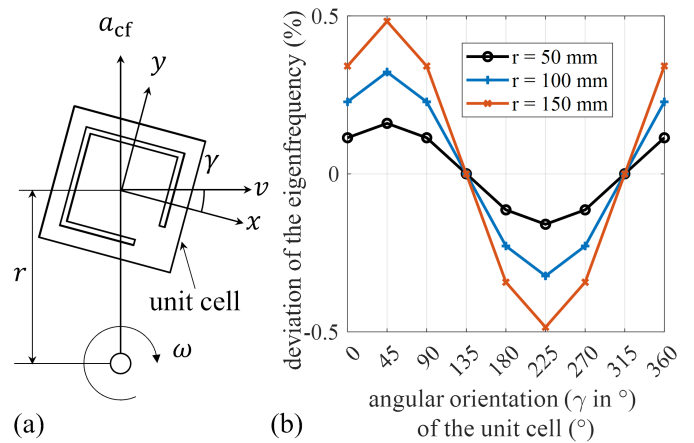


Fig. 7. Deviation of the eigenfrequency of the unit cell for different radii r and angular orientations γ of the unit cell for a rotational speed of $\omega = 300 \text{ rad/s}$. The centrifugal acceleration resulting from the speed v of the unit cell is denoted by a_{cf}

4.3. Numerical design of vibroacoustic metamaterial compound

The unit cell designed above needs to be incorporated on the saw blade in a manner that achieves a large vibration reduction and that allows the saw blade prototype to be analyzed in a rotating state by a stationary observer. To this end, there need to be circular portions on the saw blade that are not interrupted by unit cells. The chosen design of the saw blade fulfilling these requirements is depicted in Fig. 8. The circular portions, where the saw blade will be investigated experimentally by means of a laser vibrometer, are marked in grey. The 68 resonators are oriented in such a way that the spring element supporting the mass element always points in the direction of rotation. This ensures that the resonators do not catch on the workpiece if their deflection is too large. In this way, damage to the resonator array can be prevented. This is particularly important if the workpiece gets clamped by the improper use of the saw.

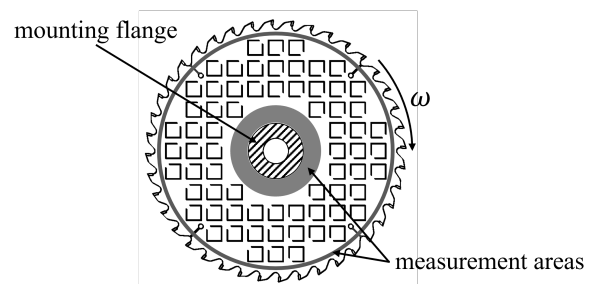


Fig. 8. Design of the saw blade with applied resonators

To validate the stop band prediction on the unit cell level for the finite saw blade with incorporated resonators as shown in Fig. 8, FE simulations were carried out. The excitation point was chosen to be the same as the one indicated in Fig. 3. For the output points, the four innermost points of Fig. 3 were chosen. The results in comparison to the already modeled saw blade behavior in Section 4.1 are depicted in Fig. 9. In good agreement with the results obtained from the unit cell, modeling the finite

system shows a stop band behavior in the frequency range of approximately 1700 – 2600 Hz. In the desired stop band frequency range, a large reduction of more than 26 dB is obtained (grey box in Fig. 9).

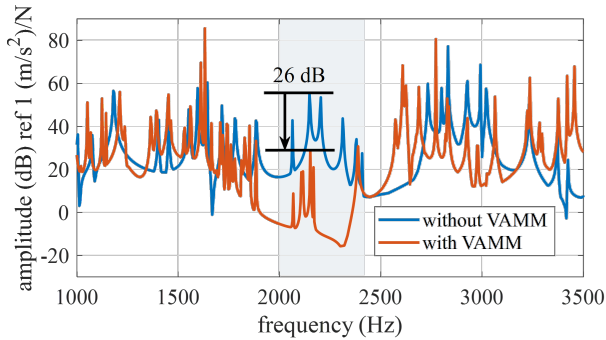


Fig. 9. Numerical stop band prediction of the finite saw blade within incorporated resonators

5. EXPERIMENTAL INVESTIGATION IN THE ROTATING STATE

A spinning disc investigated with a stationary observer shows a split in eigenfrequencies. This is because the waves travel on the disk with and in an opposite direction to the rotational speed. The following section aims to investigate whether the stop band behavior of the saw blade designed above is still present in the rotating state, even though the eigenmodes split and travel in dependence on the rotational speed.

5.1. Experimental setup

The experiments were conducted on a rotor dynamic test stand with a stationary observer in terms of a laser scanning vibrometer (Polytec PSV-300-H). The setup is shown in Fig. 10. Tests were done for the standard saw blade as well as for the one with integrated VAMM. The saw blade is mounted to an electric motor and equipped with a reflective tape of 4 mm width on the two medial diameters of 49 mm and 137 mm. The diameters for measuring were chosen based on accessibility and the boundary conditions given by the resonator array.

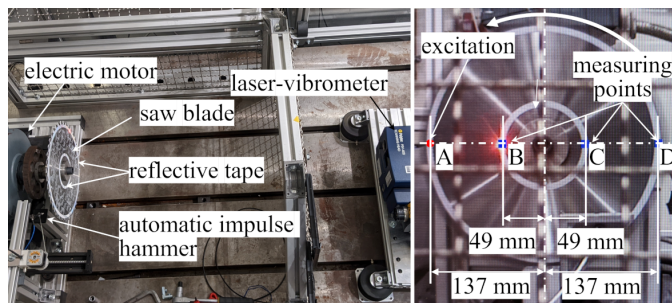


Fig. 10. Left: Test setup for measuring the surface vibrations with a laser-vibrometer in the rotating state; right: Excitation (A) and measurement points (B, C, D)

The surface velocity is measured with a stationary laser Doppler vibrometer at three points (B, C, D), as indicated in

Fig. 10, while the saw blade is spinning. The excitation is applied using a self-built automatic impulse hammer which excites the saw blade on its back side. The impulse hammer (see Fig. 11) is equipped with an acceleration sensor at the end of the hammer mass, which serves as the reference for calculating the transfer function. The hammer head together with the acceleration sensor weighs 12 g. This impulse hammer was used to prevent damage to an expensive commercial one, due to its application in a harsh environment.

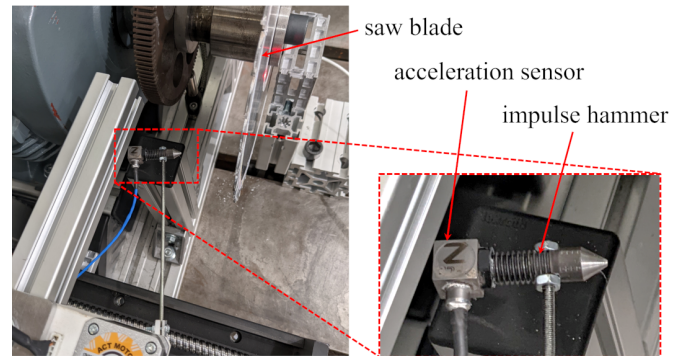


Fig. 11. Self-built automatic impulse hammer with an acceleration sensor applied to hammer head

To validate the functionality of the hammer the coherence was evaluated in the non-rotating state. The results for the three measurement points (B, C, D) for the modified and unmodified saw blades are shown in Fig. 12. To reduce the influence of the dynamics of the hammer, a force window was used. The coherence for the unmodified saw blade is close to one, with just some narrowband drops. For point D it drops to zero in between 3210 and 3325 Hz. This is outside of the desired stop band region and is therefore acceptable. The coherence for the VAMM saw blade drops within the stop band region. This is attributed to the stop band effect and already demonstrates the functionality of the VAMM. Even though vibrations are excited, they become blocked by the VAMM and cannot propagate. There-

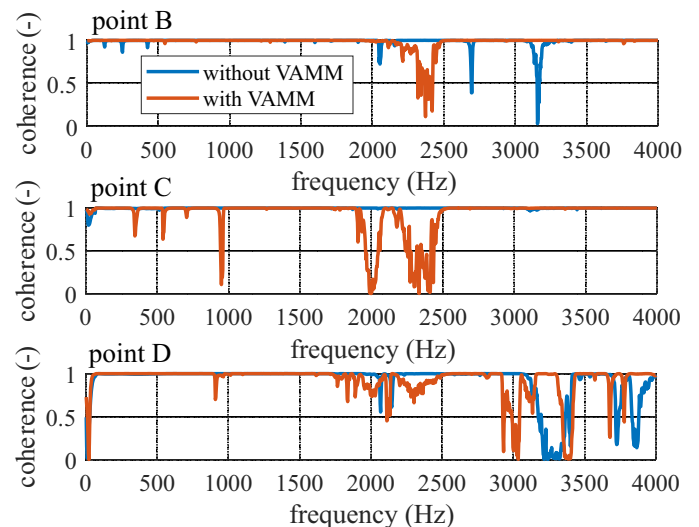


Fig. 12. Coherence of the three measurement points (B, C, D), obtained in the non-rotating state

fore, the coherence reaches low levels. The blocking of the vibrations is largest for point C since here, the vibrations must travel the longest distance through the resonator array. Point D just shows a small drop in coherence, because the vibrations do not become blocked completely and can propagate freely on the circumference of the saw blade. This behavior shows that the hammer excites accurately within the stop band frequency range.

Table 1 lists all the mode shapes present in the desired stop band region of 2000 to 2400 Hz with a margin of 100 Hz below and above this frequency range to account for numerical inaccuracies. The modeshapes are numerically obtained from the saw blade model as described in Section 4.1. Unlike the model in Section 4.1, the geometry of the mounting adapter (diameter of 60 mm) for the rotor dynamic test stand was considered. As a boundary condition for the adapter, a fixed support was chosen. All modes, as depicted in Table 1, are likely to be excited by the impulse hammer and measured with either the inner measurement points (B and C) or with the outer point D.

Table 1

Numerically obtained mode shapes of the unmodified saw blade in the stop band region from 1900 to 2500 Hz

Number	1	2	3	4	5
Mode shape					
Frequency	1928 Hz	2039 Hz	2060 Hz	2097 Hz	2110 Hz
Number	6	7	8	9	10
Mode shape					
Frequency	2180 Hz	2233 Hz	2378 Hz	2389 Hz	2408 Hz

The mode shapes at 2180 and 2233 Hz are likely not to be affected by the VAMM since the antinodes are concentrated at the circumference of the saw blade, where no resonators are placed.

5.2. Experimental results

The resulting transfer functions from the velocity of the hammer head to the velocity of the measurement point are shown in Figs 13–15 for different rotational speeds, both the standard saw blade (blue) and the saw blade with incorporated VAMM (red). Looking at the results for the inner measurement points B and C at a radius of 49 mm, the expected stop band occurs between approximately 1900 and 2500 Hz in the static case (0 rpm), which is characterized by a significant amplitude reduction. An increasing amplitude is observed in the frequency range of 2500 to 2700 Hz, following the stop band frequency range. Both effects are in line with the numerical model as shown in Section 4.3. When the rotational speed is increased, the eigenfrequencies of eigenmodes with nodal diameters of

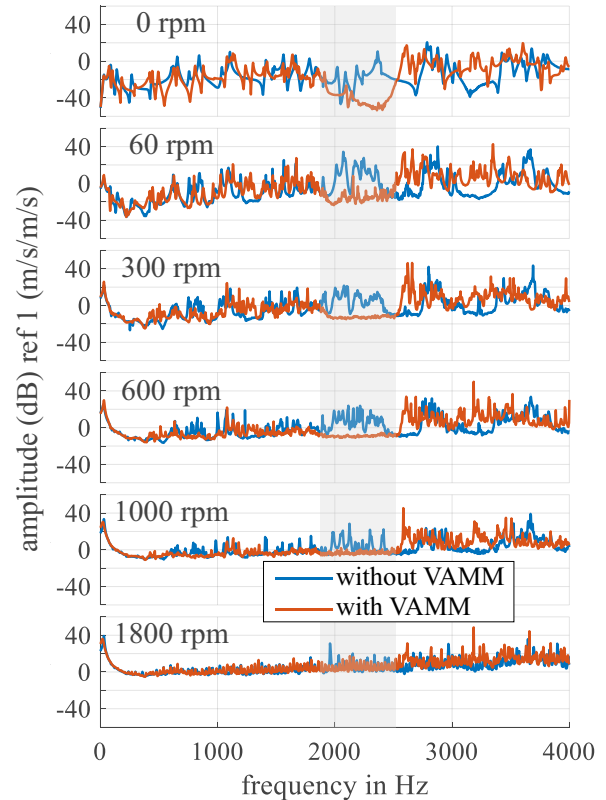


Fig. 13. Frequency response functions of measuring point B for different rotational speeds; blue: Saw blade without VAMM, red: Saw blade with VAMM

one or more split up. This effect is less well observed at measurement points B and C since they are situated close to the axis of rotation.

The effect is better visible for measurement point D because of the larger distance to the axis of rotation, as can be seen in Fig. 15. As indicated by the grey box, the stop band is still observable for rotational speeds up to 1000 rpm. At approximately 30 Hz, a distinct peak can be observed for rotational speeds above 0 rpm that is associated with the eigenfrequency of the impulse hammer, which is excited when the saw blade is spinning. This effect has no relevance to this investigation. A possibility to avoid this effect is to use a force sensor at the impulse hammer instead of the acceleration sensor.

At 1800 rpm the stop band is hardly visible due to the decreasing signal-to-noise ratio. This is likely due to the measurement principle of the laser vibrometer, which measures the surface velocity with the laser Doppler method. As the saw blade spins, the surface roughness of the reflective tape passes the measurement point at a speed dependent on the rotational speed of the saw blade. This causes the roughness to be identified as a surface velocity, which is dependent on the rotational speed. At the same time, the excitation intensity and locality of the impulse hammer are decreased. So, for the setup presented above, the investigation is limited to a rotational speed of about 1000 rpm.

The measurement results at the outer measurement point (Fig. 15) at a radius of 137 mm (point D) show slightly dif-

Vibration reduction on circular saw blades with vibroacoustic metamaterials

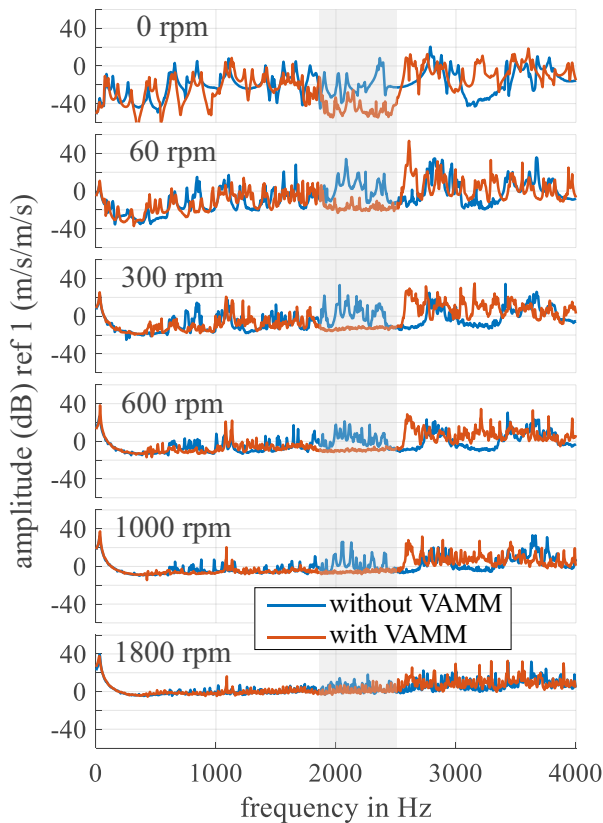


Fig. 14. Frequency response functions of measuring point C for different rotational speeds; blue: Saw blade without VAMM, red: Saw blade with VAMM

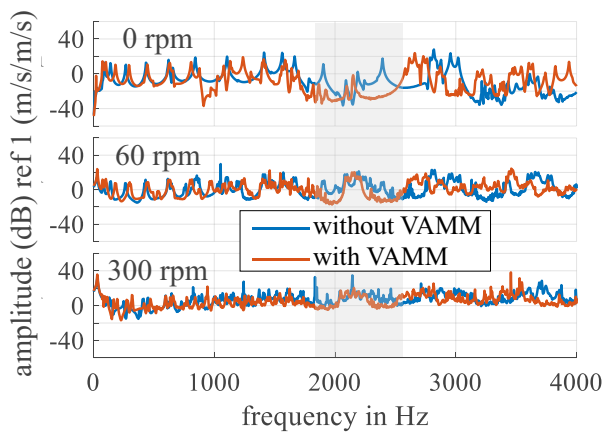


Fig. 15. Frequency response functions of measuring point D for different rotational speeds; blue: Saw blade without VAMM, red: Saw blade with VAMM

ferent effects from the ones shown in Figs. 13 and 14. Here, an amplitude reduction can also be observed for low rotational speeds between 1900 and 2500 Hz; however, the stop band effect is not as distinct as for points B and C. This is because the vibrations are induced at the same radius as the measurement takes place. In between the excitation point and the measurement point, no resonators are placed for waves that travel on the circumference of the saw blade. The two distinct peaks in-

side the stop band region are likely to be associated with modes 6 and 7 from Table 1, which feature the largest deflections in the circumference of the saw blade where no resonators are placed.

Due to the larger relative speed at a radius of 137 mm, the noise resulting from the surface roughness is larger and an investigation was only possible for rotation speeds up to 300 rpm.

6. CONCLUSIONS AND OUTLOOK

In the presented work, a VAMM suitable for integration into a saw blade was numerically designed. The stop band frequencies were chosen based on the first-order excitation frequency of the sawing process, where the largest noise emission takes place. An off-the-shelf saw blade was modified with the developed design using a water jet cutting machine. The dynamic characterization of the obtained saw blade with incorporated VAMM in comparison to the saw blade without VAMM was consecutively investigated in a non-rotating and rotating state. It is shown that the desired effect of a broadband vibration reduction in the form of a stop band for elastic waves is not only found in the dynamic characterization of the stationary blade but also occurs in the rotating system. A significant vibration reduction is observed in the frequency range of 1900 to 2500 Hz covering the desired frequency range resulting from noise measurements of the saw blade in sawing operation. This is the frequency range where the noise emission of the saw blade is the highest.

Future work will focus on the improvement of the test setup with respect to the signal-to-noise ratio so that higher rotational speeds can be used, which are closer to most application scenarios of saw blades. To achieve this, the excitation force may be enlarged or a different measurement principle (e.g., acoustical measurement) may be used. Also, rotor balancing can be performed to reduce runout, which might also cause problems in measurement. Moreover, a damped version of the blade will be manufactured and compared to the current one to reduce the amplitudes after the stop band. This may be realized by inserting a damping material into the slots of the unit cells. Furthermore, other resonator designs (using at least two spring elements supporting the mass) should be developed to account for roll tensioning, which is a common technique in saw blade manufacturing to optimize saw blade stability. Additionally, in order to avoid structural failure, the resonator design needs to be optimized to reduce stress concentrations which, with the current design, appear in the sharp corners of the cut-outs. Besides the danger of the cut-outs to the structural integrity, they also lower the axial stiffness, which influences the cutting speed and stability of the saw blade while sawing. So, another optimization accounting for this should be performed. To ensure that the deflection of the developed resonator concept during the sawing operation is small enough so that it does not interfere with the workpiece, the deflection will be measured with an optical derotator. With such a device it is possible to track a resonator with a laser vibrometer and measure its surface velocity while it is spinning during sawing.

Afterwards, the VAMM saw blade will be acoustically investigated in terms of the radiated noise during operation.

Even though the additional costs of inserting multiple slots into the sawblade are estimated to be low, investigations of the production costs will be performed. In this respect further optimization can be performed to reduce the number of resonators being cut into the saw blade, thereby reducing the production costs.

ACKNOWLEDGEMENTS

This work was supported by the Fraunhofer Internal Programs under Grant No. PREPARE 840224.

REFERENCES

- [1] F. Schelle, M. Janssen, and J. Maue, "Neuartige lärmgeminderte Sägeblätter für die Holzbearbeitung," in *Proc. 42nd Deutsche Jahrestagung für Akustik (DAGA)*, 2016, pp. 1226–1228.
- [2] A. Droba, L. Javorek, J. Svoren, and D. Paulíny, "New design of circular saw blade body and its influence on critical rotational speed," *Drewno*, vol. 58, no. 194, pp. 147–157, 2015, doi: [10.12841/wood.1644-3985.081.12](https://doi.org/10.12841/wood.1644-3985.081.12).
- [3] J. Svoren, L. Javorek, and L. Murin, "Effect of the Shape of Compensating Slots in the Body of a circular Saw Blade on Noise Level in the Cutting Process," *ProLigno*, vol. 6, no. 4, pp. 5–12, 2010.
- [4] S. Weiland and C. Birenbaum, "Optimization of geometric features of circular saw blades and parameters of the manufacturing process aided by optiSLang," in *Proc. 11th Weimarer Optimization and Stochastic Days*, 2014.
- [5] Deutsche Gesetzliche Unfallversicherung DGUV, "Geräuschgeminderte Sägeblätter für Holz, Kunststoff und Aluminium – Marktübersicht, Schalldruckpegel in Labor und Praxis, Lärmschutz-Arbeitsblatt LSA 01-375 Berufsgenossenschaftliche Informationen für Sicherheit und Gesundheit bei der Arbeit (BGI/GUV-I)." *Umwelt-online.de* [Online]. Available: [Accessed: 01. Apr. 2023].
- [6] N. Gunes Yilmaz, "Process efficiency comparison of a sandwich-core sawblade and a conventional sawblade used in stone-machining," *J. Clean Prod.*, vol. 47, pp. 26–31, 2013, doi: [10.1016/j.jclepro.2013.01.042](https://doi.org/10.1016/j.jclepro.2013.01.042).
- [7] E. Saljé and U. Bartsch, "Geräuschuntersuchung an Kreissäge- und Vorritzsägeblättern für die Holzbearbeitung," *Holz Als Roh- und Werkst.*, vol. 35, pp. 179–181, 1977.
- [8] S. Nishio and E. Marui, "Effects of slots on the lateral vibration of a circular saw blade," *Int. J. Mach. Tools Manuf.*, vol. 36, no. 7, pp. 771–787, 1996.
- [9] G. Pahlitzsch and B. Rowinski, "Über das Schwingungsverhalten von Kreissägeblättern—Dritte Mitteilung: Schwingungen der Sägeblätter im Schnitt und ihre Dämpfung," *Eur. J. Wood Prod.*, vol. 25, no. 9, pp. 348–357, 1967.
- [10] Y.M. Stakhiev, "Research on circular saw disc problems: several of results," *Holz Als Roh- und Werkst.*, vol. 61, no.1, pp. 13–22, 2003.
- [11] Berufsgenossenschaft Holz und Metall, *DGUV Information 209-044, Holzstaub*. Berlin: Deutsche Gesetzliche Unfallversicherung e.V. (DGUV), 2019.
- [12] C. Droz, O. Robin, M. Ichchou, and N. Atalla, "Improving sound transmission loss at ring frequency of a curved panel using tunable 3D-printed small-scale resonators," *J. Acoust. Soc. Am.*, vol. 145, no. 1, pp. EL72–EL78, 2019, doi: [10.1121/1.5088036](https://doi.org/10.1121/1.5088036).
- [13] S. Riess *et al.*, "Vibroacoustic Metamaterials for enhanced acoustic Behavior of Vehicle Doors," in *Proc. 15th International Congress on Artificial Materials for Novel Wave Phenomena – Metamaterials*, 2021, pp. X-374–X-376, doi: [10.1109/Metamaterials52332.2021.9577065](https://doi.org/10.1109/Metamaterials52332.2021.9577065).
- [14] S. Riess, M. Droste, S. Shariatinia, and H. Atzrodt, "Design of Vibroacoustic Metamaterial for vibration Reduction on Sheet Metal Structures for Industrial Machinery," in *Proc 16th International Congress on Artificial Materials for Novel Wave Phenomena – Metamaterials*, 2022, pp. X-359–X-361, doi: [10.1109/Metamaterials54993.2022.9920821](https://doi.org/10.1109/Metamaterials54993.2022.9920821).
- [15] A. Mondal, S. Dutta, and S. Murugan, "Coupled flexural and torsional vibration attenuation with locally resonant metamaterials," *Mater.Today-Proc.*, vol. 87, pp. 99–103, 2023, doi: [10.1016/j.matpr.2023.01.111](https://doi.org/10.1016/j.matpr.2023.01.111).
- [16] I. Arretche and K.H. Matlack, "Centrifugal forces enable band gaps that self-adapt to synchronous vibrations in rotating elastic metamaterial," *Mech. Syst. Signal Proc.*, vol. 202, p. 110689, 2023, doi: <https://doi.org/10.1016/j.ymsp.2023.110689>.
- [17] C. Rosso, E. Bonisoli, and F. Bruzzone, "On the Implementation of Metastructures in Rotordynamics," in *Rotating Machinery, Vibro-Acoustics & Laser Vibrometry, vol. 7. Conference Proceedings of the Society for Experimental Mechanics Series*, D. Di Maio, Ed., 2018, doi: [10.1007/978-3-319-74693-7_5](https://doi.org/10.1007/978-3-319-74693-7_5).
- [18] S. Riess, M. Droste, and H. Atzrodt, "Noise Reduction of circular Saw Blades using Vibroacoustic Metamaterial," in *Proc. 16th International Congress on Artificial Materials for Novel Wave Phenomena – Metamaterials*, 2022, pp. X-362–X-364, doi: [10.1109/Metamaterials54993.2022.9920757](https://doi.org/10.1109/Metamaterials54993.2022.9920757).
- [19] F. Bloch, "Über die Quantenmechanik der Elektronen in Kristallgittern," *Zeitschrift für Physik*, vol. 52, pp. 555–600, 1929.
- [20] C. Claeys, "Design and Analysis of Resonant Metamaterials for Acoustic Insulation," Ph.D. dissertation, KU Leuven, Belgium, 2014.
- [21] H. Al Ba'ba'a, M.A. Attarzadeh, and M. Nouh, "Experimental Evaluation of Structural This work was supported by the Fraunhofer Internal Programs under Grant No. PREPARE 840224. Intensity in Two-Dimensional Plate-Type Locally Resonant Elastic Metamaterials," *J. Appl. Mech.*, vol. 85, no. 4, pp. 041005-1–041005-9, 2018, doi: [10.1115/1.4039042](https://doi.org/10.1115/1.4039042).